AMR Infrastructure Expansion, Adding Complexity

Roy Stogner

roystgnr@cfdlab.ae.utexas.edu

Univ. of Texas at Austin

January 12, 2007

CFDLab

Outline

CFDLab

Boundary Value Problem Framework Goals

Goals:

- Improving test coverage and reliability
- Hiding of implementation details from user code
- Rapid prototyping of differential equation approximations
- Improved error estimation

Methods:

- Object-oriented System and Solver classes
- Numerical Jacobian verification

FEM System Classes

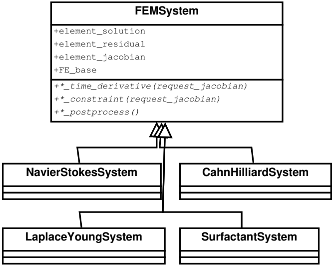

- Generalized IBVP representation
- FEMSystem does all initialization, global assembly
- User code only needs weighted time derivative residuals $(\frac{\partial u}{\partial t}, v_i) = F_i(u)$ and/or constraints $G_i(u, v_i) = 0$

ODE Solver Classes

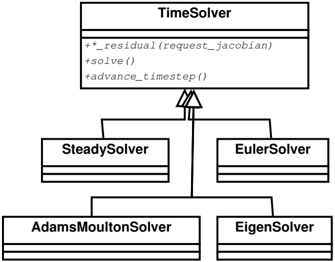

- Calls user code on each element
- Assembles element-by-element time derivatives, constraints, and weighted old solutions

Nonlinear Solver Classes

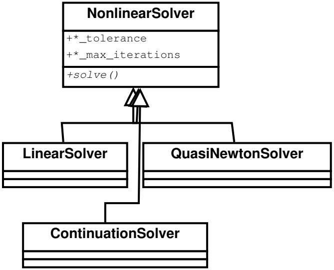

- Acquires residuals, jacobians from FEMSystem assembly
- Handles inner loops, inner solvers and tolerances, convergence tests, etc

Element-based BVP Framework

Pros:

- Enables non-global physics-based error estimators
- Removes dependencies, complications from application level
- Gives user access to more tested code
- Enables element-by-element Jacobian verification

Cons:

- Adds additional per-element virtual function calls
- Complicates time-dependent stabilization methods
- Complicates operator splitting methods

C^1 Finite Element Spaces

In Galerkin formulations of plate bending, streamfunction viscous flow, Cahn-Hilliard interfaces, and surface tension driven films, we find integrated products of second derivatives of the solution and test functions.

With variational problems posed on subspaces of $H^2(\Omega)$, conforming finite element approximations require H^2 conforming functions.

A C^1 continuous (and $W^{2,\mathrm{inf}}$ bounded, $W^{2,p}$ conforming) finite element is needed, e.g.:

- Powell-Sabin 6-split triangle
- Powell-Sabin-Heindl (PSH) 12-split triangle
- Hsieh-Clough-Tocher (HCT) 3-split triangle

Macroelements

Constraining polynomial triangles to C^1 continuity requires quintic polynomials. To use lower p, we construct macroelements by subdividing each triangle, using piecewise polynomial functions with continuity constraints along interior edges.

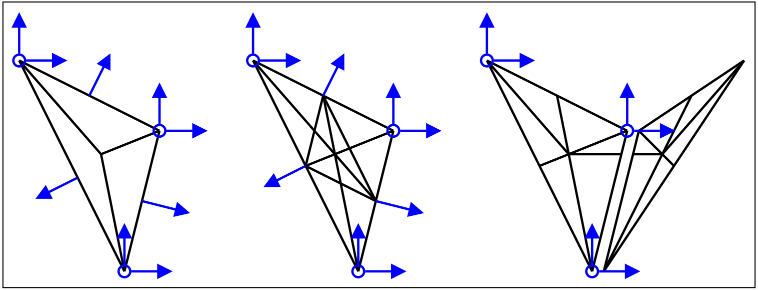

CFDLab

Approximation Convergence

PSH and HCT triangles exactly reproduce quadratics and cubics $(k \equiv 2, 3)$, respectively. Standard interpolation, H^2 approximation rules apply for $w \in H^n(\Omega) \subset H^{k+1}(\Omega)$, but L_2 approximation on PSH triangles is suboptimal.

$$
\begin{aligned}
||w - P_h w||_{H^m(\Omega)} &\leq Ch^{n-m} \, |w|_{H^n(\Omega)} \\
||u - u_h||_{H^2(\Omega)} &\leq Ch^{n-2} \, ||u||_{H^n(\Omega)} \\
||u - u_h||_{H^r(\Omega)} &\leq Ch^{\min(2(k+1-m), k+1-r, n-r)} \, ||u||_{H^n(\Omega)}
\end{aligned}
$$

CFDLab

Adaptive h Constraints

Constraining hanging degrees of freedom can be more difficult on general non-hierarchic bases

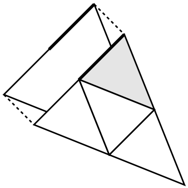

$$
\begin{aligned}
u^F &= u^C \\
\sum_i u_i^F \phi_i^F &= \sum_j u_j^C \phi_j^C \\
A_{ki} u_i &= B_{kj} u_j \\
u_i &= A_{ki}^{-1} B_{kj} u_j
\end{aligned}
$$

Integrated values (and fluxes, for C^1 continuity) give element-independent matrices:

$$
\begin{aligned}
A_{ki} &\equiv \left(\phi_i^F, \phi_k^F\right) \\
B_{kj} &\equiv \left(\phi_j^C, \phi_k^F\right)
\end{aligned}
$$

Adaptive p Constraints

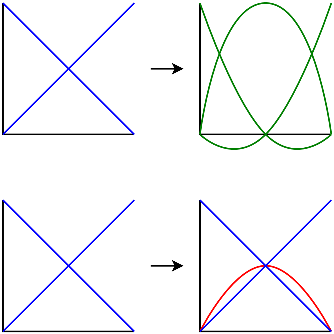

- p refinement is well suited to hierarchic adaptivity
- Hanging degree of freedom coefficients are simply set to 0

Error Indicators

Integration by parts gives an upper error bound on subelements S for the biharmonic problem:

$$\begin{aligned} ||e||_{H^2(\Omega)} \quad &\leq \quad C_\Omega \sum_S \Big[||f - \Delta^2 u_h||_S \, h_S^2 + \\ & \frac{1}{2} \, ||[[\partial_{\vec{n}} \Delta u_h]]||_{\partial S} \, h_S^{3/2} + \frac{1}{2} \, ||[[\Delta u_h]]||_{\partial S} \, h_S^{1/2} \Big] \end{aligned}$$

The most significant term gives a simple indicator on elements K for more general fourth order problems:

$$\eta_K \equiv \sqrt{h_K} \, ||[[\Delta u_h]]||_{\partial K}$$

CFDLab

Diffuse Interface Modeling with AMR/C

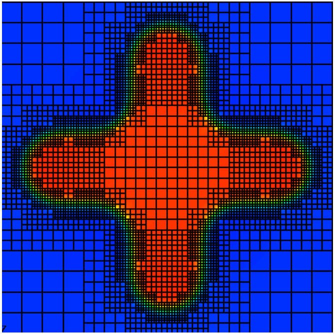

- Mesh coarsening in smooth regions is traded for mesh refinement in sharp layers
- Equivalent accuracy is achieved here with 75% fewer degrees of freedom than a uniform mesh

Diffuse Interface Modeling with AMR/C

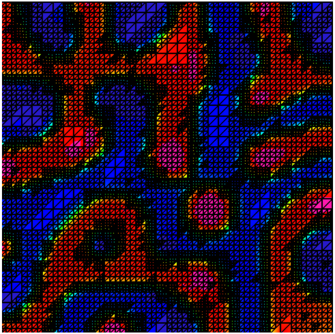

- Adaptive Mesh Refinement / Coarsening reduces solver expense
- Laplacian Jump error indicator tracks moving interfaces

CFDLab

Adaptive Refinement Strategies

Maintaining a constant global error estimate:

- Tracks time-varying complexity
- Gives reliable results
- Requires reliable error bounds

Maintaining constant element count:

- Keeps an upper bound on computational expense
- Only requires a good feature indicator

CFDLab

Microscale and Nanoscale Applications

Cahn-Hilliard phase decomposition can model such disparate phenomena as:

- Tin-Lead solder aging
- Void lattice formation in irradiated semiconductors
- Self-assembly of thin film patterns

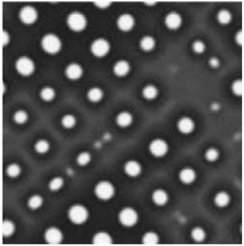

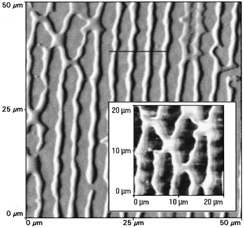

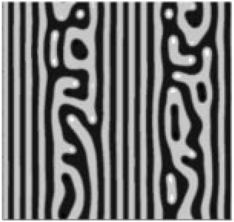

Free Energy Formulation

Cahn-Hilliard systems model material separation and interface evolution by tracking flow driven by configurational and interfacial free energy minimization.

$$
\begin{aligned}
f_0(c) &\equiv \frac{1}{4}\left(c^2-1\right)^2 \\
f_\gamma(\nabla c) &\equiv \frac{\epsilon_c^2}{2}\nabla c \cdot \nabla c
\end{aligned}
$$

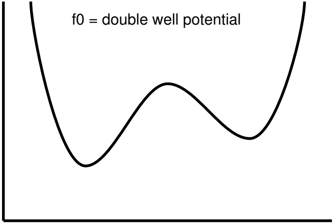

Cahn-Hilliard Equation

Adding a material-dependent mobility coefficient defines the concentration flux.

$$
\begin{aligned}
\vec{J} &= M_c \nabla \frac{df}{dc} \\
&= M_c \nabla \left(f_0'(c) + f_\gamma'(c) \right) \\
&= M_c \nabla \left(c^3 - c - \epsilon_c^2 \Delta c \right)
\end{aligned}
$$

$$
\frac{\partial c}{\partial t} = \nabla \cdot M_c \nabla \left(c^3 - c - \epsilon_c^2 \Delta c \right)
$$

CFDLab

Weak Cahn-Hilliard Equation

Taking a weighted residual and integrating by parts twice,

$$
\begin{aligned}
\left(\frac{\partial c}{\partial t}, \phi\right)_\Omega \quad = \quad & -\left(M_c \nabla \left(c^3 - c\right), \nabla \phi\right)_\Omega - \epsilon_c^2 \left(\Delta c, \nabla \cdot M_c^T \nabla \phi\right)_\Omega \\
& + \left(\left(M_c \nabla \left(c^3 - c - \epsilon_c^2 \Delta c\right)\right) \cdot \vec{n}, \phi\right)_{\partial\Omega} \\
& + \epsilon_c^2 \left(\Delta c, M_c^T \nabla \phi \cdot \vec{n}\right)_{\partial\Omega}
\end{aligned}
$$

Gives a functional defined on $W^{2,2}(\Omega) \cap W^{1,4}(\Omega)$ in case of constant M_c.

CFDLab

Phase Separation

- Random perturbations in initial conditions rapidly segregate into two distinct phases, divided by a labyrinth of sharp interfaces
- Rapid anti-diffusionary process

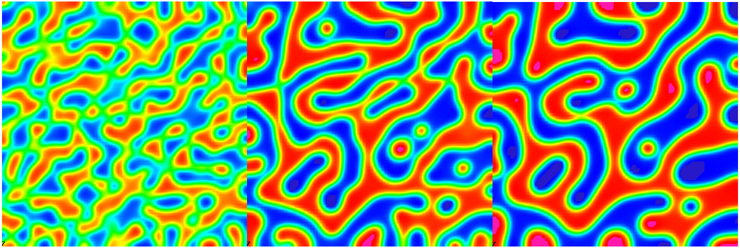

CFDLab

Spinodal Decomposition

- Over long timescales, single-phase regions coalesce
- Motion into curvature vector resembles surface tension
- Patterning may occur when additional stress, surface tropisms are applied

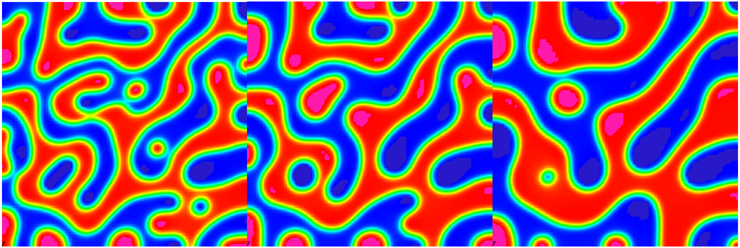

CFDLab

3D Phase Separation

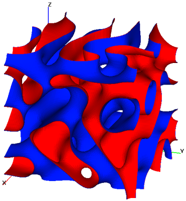

- Qualitatively similar
- Topologically very different
- Much more computationally intensive

Thin Film Patterning

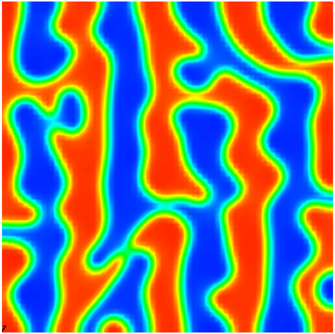

- Electrostatic or chemical surface treatment attracts one material component preferentially
- A spatially varying bias is added to the configurational free energy

CFDLab

Effects of Bias Strength

Low surface potential energy biases are overwhelmed by random noise

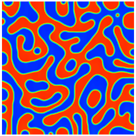

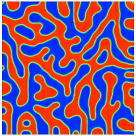

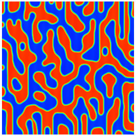

Effects of Bias Strength

Higher surface potential energy biases form patterns with decreasing defect density

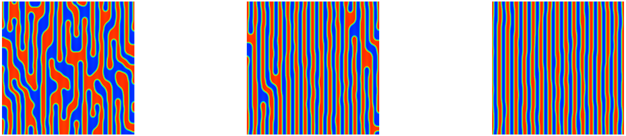

References

B. Kirk, J. Peterson, R. Stogner and G. Carey, “libMesh: a C++ library for parallel adaptive mesh refinement/coarsening simulations”, *Engineering with Computers*, in press

R. Stogner and G. Carey, “C^1 macroelements in adaptive finite element methods”, *Int. J. Num. Meth. Eng.*, in press

R. Stogner, B. Murray, and G. Carey, “Parallel approximation of Cahn-Hilliard systems in adaptive C^1 finite element spaces”, in progress

CFDLab